SATELLITE-BASED DETECTION OF OIL SPILL SIGNATURE RESIDUAL USING SYNERGY MULTISPECTRAL IMAGES OF LANDSAT-8 OLI AND LANDSAT-7 ETM+

Jamal Jasim Abdulla Althawadi (1)(2), Mazlan Hashim(1)(2)(*)

[1]Geoscience & Digital Earth Centre (INSTEG), Research Institute for Sustainable Environment (RISE), Universiti Teknologi Malaysia, Johor Bahru, Malaysia

[2]Faculty of Built Environment & Surveying, Universiti Teknologi Malaysia, Johor Bahru, Malaysia

*corresponding author: E-Mail mazlanhashim@utm.my

ABSTRACT: Satellite-based detection of oil spills is essential as it assists in reducing the risk of disasters occurring in the ocean environment to protect and reduce economic losses. The visible bands of Landsat-8 OLI and Landsat-7 ETM+ is a crucial means for detecting ocean oil spills that cause grave damage to the maritime ecosystem. Therefore, this study used the synergy of Landsat images to identify the residual oil spills along the Arabian Gulf region. Feature-based detection techniques by employing both region and point-based were adopted to compare with the multi-sensor's spatial-resolutions for detecting the oil spills. These multi-sensor data were used to extract the spill-pixels for signature's analyses. The variants against spill signatures were distinguished through calibration analysis. Results revealed that the pre-processed, as well as atmospherically corrected signatures of the spill, are reasonably agreed with the occurrence of spill records, demonstrating a high correlation ($R^2 > 0.85$, $p < 0.001$). The calibration matrices have been formulated to calibrate spill pixels for Landsat-8 OLI and Landsat-7 ETM+, which serves as a crucial input for oil spill monitoring system against local uncertainties from look-alikes. Hence, this study will attribute in fast-tracking 2025 agenda of target 14.1 (reduce marine pollution) of sustainable development goal 14th set by United Nation.

KEYWORDS: Multi-sensor, calibration, 2025 agenda

1. INTRODUCTION

Remote sensing application has been documented in monitoring and detection of oil spill, classification between false positive and positive values and simulation of oil impacts on natural ecosystem of the coastal are by number of authors (Setiawan, et al., 2017; Lu, et al., 2016; Pisano, et.al., 2015).

Satellite-based oil spills detection and tracking has undergone remarkable advances. The most significant of these studies ranges from the visible, shortwave to thermal infrared (optical), and the microwave radar bands. The ability to characterize the uniqueness emanating from the interactions of incident energy on spills are the key elements in detecting the spill in both optical and radar bands. The sea/ocean surfaces conditions and the corresponding local weather systems produces large variations in resultant signatures of spills. The differences within the signature of the spill causes high uncertainties in delineating between spills and look-alikes. Researchers have focused their studies on detection and mapping spills against the background (Garcia-Pineda *et al.*, 2017; Mullin, 2017; Topouzelis, 2008). These are rather relative analysis of spills signatures against the lookalikes and backgrounds. The previous studies did not addressed the uniqueness of oil spills at absolute level, neither did they report the vectors of the spills against background targets.

Fresh occurrence starts at time of spills, the characteristics of its viscosity and floating of the spill above water surface, depends on the volume and the surrounding environmental factors such as wind velocity. Previous studies of Cheng *et al.* (2011); Guo, (2017) and Spaulding, (2017) used models to address evironmental dynamics of spills, however, they did not address the characteristics of the spill signatures interactions within the environment. Extracting oil spill signatures using remote sensing (RS) is a progressive process and an evergreen study (Bhangale *et al.*, 2017; Fiscella *et al.*, 2000). Satellite-based RS for oil spill monitoring based on medium-resolution data of MODIS, infrared, hyperspectral, multi-source, multi-temporal and multispectral, as well as radar data have

adequately been explored by previous studies. Therefore, in this study, the spectral signatures of oil spills using various optical-based medium-resolution satellites data, such as; Landsat-7 ETM+, and Landsat-8are investigated. In order to identify the variants within signatures of the oil spills around Arabian Gulf. Multi-satellite sensors were used for pre-processing and producing the complete signatures matrix, which is very essential for calibration of all the satellite-based oil spill-leaving reflectance.

2. MATERIALS AND METHOD

2.1 Study Area

The study area is the Arabian Gulf, Located between Arabian Peninsula and southwestern Iran (Figure 1). Covering a sea area of about 241,000 km^2 with 990 km total length and width range from 55km to 340km (Powers *et al.*, 1966). It is boarded by Kuwait, Saudi Arabia, Bahrain, Qatar, United Arab Emirates, Iraq, Oman and Iran. The spills considered in this study occurred between January 2016 to January 2018. The spill records were compiled by Marine Emergency Mutual Aid Centre (MEMAC). 7 major spill locations designated as A to G as shown in Figure 1. Landsat-7 ETM+, and Landsat-8 OLI satellite image were extracted from each location to show the spills area. Spill areas ranged from 800-50,000 pixels in area. They were of various shapes mostly influenced by local wind and current conditions.

Figure 1. Study area – Arabian Gulf.

2.2 Satellite Data

Table 1 shows the details of the sets of satellite data used in this study (Landsat-7 ETM+, and Landsat-8 OLI. The data were acquired during spill occurrences as indicated below (Figure 2). Whereas, the sea-truths for oil spill occurrences records and look-likes were obtained from the records of maritime notices and costal authorities of the area.

Table 1. Date of satellite imagery used for oil detection in Arabian Gulf

Location	Date of oil spill	Landsat 7 ETM+	Landsat 8 OLI
Al-Khafji	9/5/2016	18/5/2016	10/5/2016
Iran	9/10/2016	11/10/2016	19/10/2016
Zour	10/8/2017	18/8/2017	17/8/2017
Darius	8/8/2017	18/8/2017	10/8/2017
Al-Arabiyah	26/9/2017	28/9/2017	27/9/2017
Safa Oilfield	25/8/2017	27/8/2017	26/8/2017
Sirri Island	7/9/2017	7/9/2017	15/9/2017

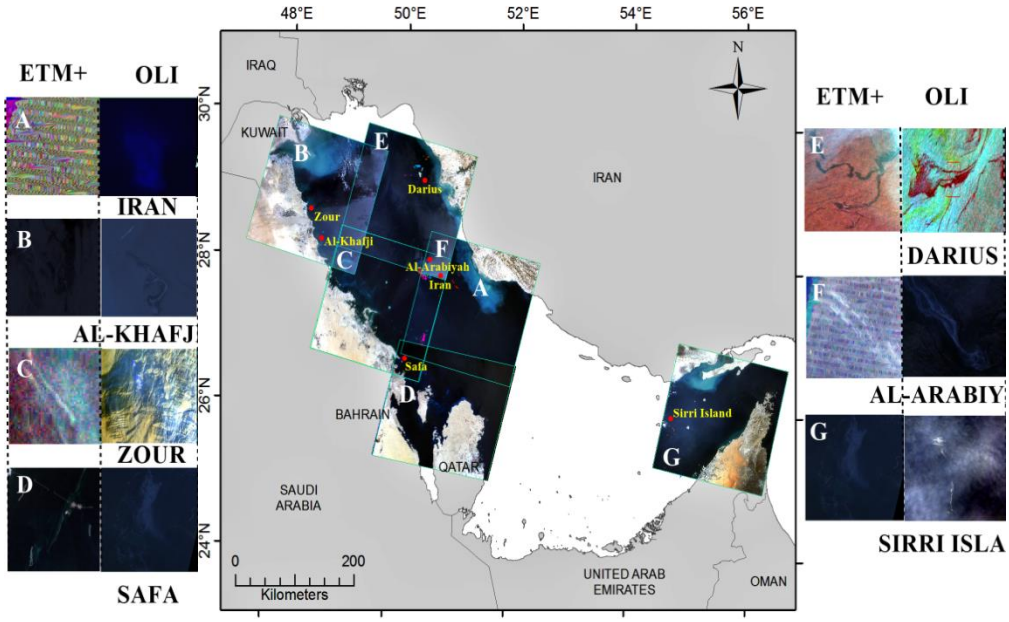

Figure 2. oil spills occurrences 2016-2017. Scene boundary line between all satellite images selected and used in this study.

2.3 Satellite Data Processing

Radiometric, atmospheric and geometric corrections were used to pre-process the satellite images. The spill features were extracted, and the related signature analysis carried out in the data processing stage. Image subset and image masking were performed to reduce all geometric misrepresentations inherent in the image. The image was geo-referenced to the UTM coordinate system, datum WGS-84 area 48N using a set of ground control points (GCP) identifiable both in the satellite. Digital map of the study area was used as reference to correct geometric distortion

of images. The resampling schemes of nearest neighbor were finally selected to convert all pixel brightness recorded in digital number (DN) from raw images to ensure slight radiometric changes.

In order to minimization scattering effects on adjacent pixels, an atmospheric correction of these image set was performed. The algorithm of the atmospheric correction for all the spectral bands of images used and FLAASH program of the ENVI V5 software used is presented in equation 1.

$$Li = \left(\frac{A_{\rho}}{1 - \rho_e S} \right) + \left(\frac{B\rho_e}{1 - \rho_e S} \right) + L_a \qquad (1)$$

where:

L_i = the spectral radiance at sensor pixel;
ρ = the pixel surface reflectance;
ρ_e = an average surface reflectance for the pixel and a surrounding region;
S = the spherical albedo of the atmosphere;
L_a = the radiance back scattered by the atmosphere; and
A and B = coefficients that depend on atmospheric and geometric conditions but not on the surface.

The radiometric correction method was used to convert the digital value in all pixels into reflectance of radiance unit. Landsat ETM+, and Landsat OLI have mathematic model to convert the pixel. In contrast, to Landsat ETM+, and Landsat OLI image can directly convert its DN to reflectance value (L_λ). The rescaling improvements and biases for Landsat 8 OLI satellite data were obtained following:

$$\rho_\lambda' = M\rho Qcal + A_{p\ AL} \qquad (2)$$

where:

ρ_λ' = TOA spectral radiance (Watts/ (m^2 * srad * μm));
$M\rho$ = Band-specific multiplicative rescaling factor from the metadata;
$A\rho$ = Band-specific additive rescaling factor from the metadata; and
Q_{cal} = Quantized and calibrated standard product pixel values (DN).

Finally, the spill signatures within the spectral band were determined by extracting all spill pixels using both spatial and feature based entities. The calibration tool of Landsat ETM+ in ENVI software was used to extract the DN of pixel for Landsat ETM. The region-based segmentation technique in ENVI system was used to extract all pixels by initiating seed points to identify the locations of spill as reported in the supplementary information of the respective 7 locations. The generated spill sections are shown in the inset of Figure 2 (A – G), whereas, summary of the spill's locations is presented in Table 2.

Table 2. Summary of spills identified based on regions grown from satellite images by initial seed points located at location of reported spill occurrences.

Location	Landsat-7 ETM+		Landsat-8 OLI	
	Total pixel	Area (km^2)	Total pixel	km^2
Iran	1,033	0.92	8,106	7.3
Al-Arabiyah	5,271	4.74	51,492	46.34
Zour	222	0.2	3,470	3.12
Darius	9,519	8.57	6,508	5.86
Alkhafji	98	0.09	853	0.77
Safa	810	0.73	55,887	50.3
Sirri	17,786	16.01	2,091	1.88

3. RESULTS & DISCUSSION

The The signatures of the spills from all the visible bands of the satellite image sets were grouped into 3 major spectral visible regions of red (R), green (G) and blue (B). The average of each spill events extracted from all the signatures for each located were recorded in the 3 spectral regions according to the sensor systems. Hence, 3 sets of RGB signatures for ETM+, and OLI were applied in this study.

To analyze the results, the variants of the signatures RGB spectral bands were plotted as a function of the corresponding spectral responses record of oil slick film over seawater (Clark, *et al.*, 2010). Figure 2 shows the variations of the comparator spectra marked as in-situ reflectance. Each column (left to right) represents signatures of Landsat-7 ETM+, and Landsat-8 OLI. The rows from top to bottom represents the blue, green and red spectral regions. The R^2 of the linear regression reported at 0.001 significant level showed consistence ranges of 0.79 – 0.99, and 0.72- 0.86 for ETM+, and OLI, respectively. From the results shows clear indication of consistencies in the processed satellite-derived signatures. The blue signatures showed more variants compared to green and red, this could as a result of intricateness of the interaction between the incoming solar radiation and the surface targets (spills, and water surface background). Scattering effects was also higher theoretically within blue spectral region compared to green and red. The least variation is in red, which was observed with R^2 of more than 0.86. The result has therefore, contribution significantly in reporting the absolute oil spill signatures within visible bands for the region (Arabian Gulf). The on-going works for the entire spectral region including near infra-red and thermal infrared regions. Without these absolute signatures indicators of spill, a monitoring spill system would be based on relative analysis, which is risky in reporting the look-alikes. This research has produced a full spectral library of spills of the area under study which can now be used to anticipate for high certainty future spill monitoring system.

The information derived from these signature variations reported was used to create a calibration matrix for spill calibrations obtained from images (ETM+, and OLI) such that:

$$\begin{bmatrix} R_{ETM} \\ G_{ETM} \\ B_{ETM} \end{bmatrix} = [R_i \quad G_i \quad B_i]. \begin{bmatrix} 0.3662 \\ 1.0642 \\ 5.0216 \end{bmatrix} + \begin{bmatrix} 0.0126 \\ -0.0137 \\ -0.0603 \end{bmatrix} \qquad (3)$$

$$\begin{bmatrix} R_{OLI} \\ G_{OLI} \\ B_{OLI} \end{bmatrix} = [R_i \quad G_i \quad B_i] \begin{bmatrix} 2.2482 \\ 1.6630 \\ 7.5500 \end{bmatrix} + \begin{bmatrix} -0.1479 \\ -0.0044 \\ -0.1222 \end{bmatrix} \qquad (4)$$

where:

R_{ETM}, G_{ETM}, B_{ETM} are calibrated ETM bands in red, green and blue spectral region,

R_{OLI}, G_{OLI}, B_{OLI} are calibrated OLI bands in red, green and blue spectral region,

R_i, G_i and B_i are spill pixels within red, green and blue spectral region,

The coefficients for R_i, G_i and B_i are gains for red, green and blue spectral region, and

The constants in last matrix term are the offsets for red, green and blue spectral region.

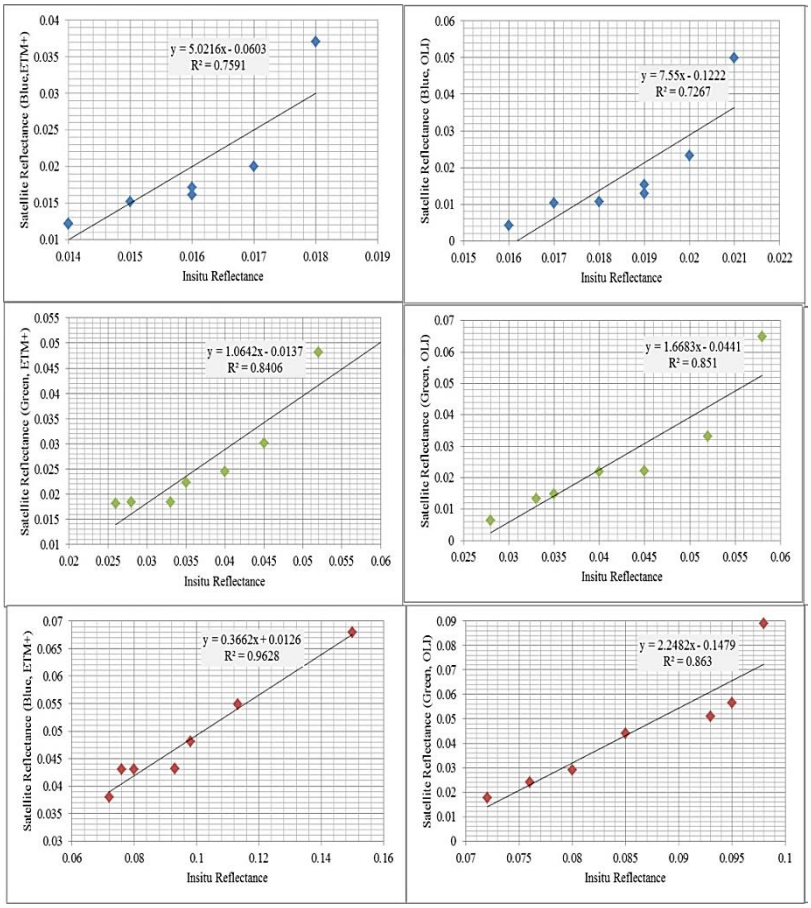

Figure 2. Variations of means-of-spill signatures from 7 occurrences against spill signatures of NASA (Clark, *et al.*, 2010). Each column (left to right) represents signatures of Landsat-7 ETM+, and Landsat-8 OLI. The row (top to bottom) represents the blue, green and red spectral regions.

The signature calibration matrix formulated and the related novel concept could be useful inputs in the extraction of absolute spills signatures within the known spectral regions irrespective of satellite system used. And the matrices can also provide ready-ingest for rigorous computational aspects in the digital image processing of the system.

The final assessment of the calibrated signatures spill pixels in Al-khafji (Site B in Fig. 1) for significant tests for:

(i) T-test for Ho : the calibrated spill pixels treated using matrices of (3), (4) for ETM+, and OLI is comparable to standard in-situ oil film signatures in Red, Blue and Green bands; and

(ii) F-test for Ho: the variation of treated spill pixels is similar to the variation of standard in-situ oil film signatures in Red, Blue and Green bands (Table 3). The results indicate acceptance of similar mean and variations. This confirms the applicability of these matrices for spill signatures calibration at absolute spectral values.

Table 3. Summary of significant tests for mean and variance of spill signatures treated with calibrated matrices.

	t-Test	F-test	P	inference
Landsat ETM+	0.000935	0.000320	0.005	Accept Ho
Landsat OLI	0.073551	0.150965	0.005	Accept Ho

4. CONCLUSION AND FUTURE DIRECTION

Variations within oil spill signatures for Arabian Gulf which occurred between 2016-2017 within this period, 7 reported major spill locations, were highlighted. The emphasis on these variations against standard signature of oil film over water within visible spectral bands was reported. This study has shown the requirements of the appropriate digital image processing and treatment to enable absolute signatures derived without any uncertainties. These signature variations were used to formulate calibration matrices for spills identified from satellite images, which can be used for processing of spill monitoring system. This study will attribute in fast-tracking 2025 agenda of target 14.1 (reduce marine pollution) of sustainable development goal 14th set by United Nation.

Acknowledgments

Acknowledgments of research facilities used at Universiti Teknologi Malaysia, with grant supports from supports from MOHE grants: Blue Carbon Seagrass Mapping with Remote Sensing (R.J130000.7809.4F854); and HABs Physiological Ecology Identification using Multi-mission satellite observations (R.J130000.7809.4L851).

Reference

Bhangale, U., Durbha, S. S., King, R. L., Younan, N. H. and Vatsavai, R., 2017. High performance GPU computing based approaches for oil spill detection from multi-temporal remote sensing data. Remote Sensing of Environment, PP. 202, 28-44.

Cheng, Y., Li, X., Xu, Q., Garcia-Pineda, O., Andersen, O. B. and Pichel, W. G., 2011. SAR observation and model tracking of an oil spill event in coastal waters. Marine pollution bulletin. 62(2), pp. 350-363.

Clark, R. N., Swayze, G. A., Leifer, I., Livo, K. E., Kokaly, R., Hoefen, T., Lundeen, S., Eastwood, M., Green, R. O. and Pearson, N., 2010. A method for quantitative mapping of thick oil spills using imaging spectroscopy. US Geological Survey Open-File Report. 1167(2010), pp. 1-51.

Fiscella, B., Giancaspro, A., Nirchio, F., Pavese, P. and Trivero, P., 2000. Oil spill detection using marine SAR images. International Journal of Remote Sensing. 21(18), pp. 3561-3566.

Garcia-Pineda, O., Holmes, J., Rissing, M., Jones, R., Wobus, C., Svejkovsky, J. and Hess, M. (2017). Detection of Oil near Shorelines during the Deepwater Horizon Oil Spill Using Synthetic Aperture Radar (SAR). Remote Sensing. 9(6), pp. 567.

Guo, W., 2017. Development of a statistical oil spill model for risk assessment. Environmental Pollution, pp. 230, 945-953.

Lu, Y., Sun, S., Zhang, M., Murch, B., & Hu, C., 2016. Refinement of the critical angle calculation for the contrast reversal of oil slicks under sunglint, *Journal of Geophysic.* Research. Oceans, 121, 148–161, doi:10.1002/2015JC011001.

Mullin, J. V., 2017. Advances from Arctic Oil Spill Response Research. Proceedings of the 2017 International Oil Spill Conference Proceedings: International Oil Spill Conference. 1487-1506.

Pisano, A., Bignami, F., & Santoleri, R., 2015. Oil Spill Detection in Glint-Contaminated Near-Infrared MODIS Imagery. *Remote Sensing*, *7* (1), 1112–1134. MDPI AG. Retrieved from http://dx.doi.org/10.3390/rs70101112'.

Powers, R., Ramirez, L., Redmond, C. and Elberg, E., 1966. Geology of the Arabian Peninsula. Geological survey professional paper, PP. 560, 1-147.

Roy, D. P., Ju, J., Lewis, P., Schaaf, C., Gao, F., Hansen, M. and Lindquist, E., 2008. Multi-temporal MODIS–Landsat data fusion for relative radiometric normalization, gap filling, and prediction of Landsat data. Remote Sensing of Environment. 112(6), pp 3112-3130.

Setiawan, A., Putri, M.R., Gade, M., Pohlmann, T., & Mayer, B., 2017. Combining ocean numerical model and SAR imagery to investigate the occurrence of oil pollution, a case study for the Java Sea. IOP Conf. Series: Earth and Environmental Science, 54, 012080 doi:10.1088/1755-1315/54/1/012080.

Spaulding, M. L., 2017. State of the art review and future directions in oil spill modeling. Marine pollution bulletin. 115(1-2),pp. 7-19.

Toming, K., Kutser, T., Laas, A., Sepp, M., Paavel, B. and Nõges, T., 2016. First experiences in mapping lake water quality parameters with Sentinel-2 MSI imagery. Remote Sensing. 8(8),pp. 640.

Topouzelis, K. N.,2008. Oil spill detection by SAR images: dark formation detection, feature extraction and classification algorithms. Sensors. 8(10),pp. 6642-6659.